ISSN 0023-1584, Kinetics and Catalysis, 2025. © Pleiades Publishing, Ltd., 2025.

Enhanced Acrylic Acid Production via Liquid-Phase Glycerol Oxydehydration Using SBA-15 Supported Heteropoly Phosphotungstic Acid Catalysts: Experimental Evaluation, Mechanistic Understanding, and Kinetic Modelling

Muhammad Yusri Ahmad[a, b], Syamima Nasrin Mohamed Saleh[b, *], Anwar Ul-Hamid[c], and Ahmad Zuhairi Abdullah[a, **]

[a] *School of Chemical Engineering, Universiti Sains Malaysia, Nibong Tebal, Penang, 14300 Malaysia*

[b] *Department of Chemical Engineering and Energy Sustainability, Faculty of Engineering, Universiti Malaysia Sarawak, Kota Samarahan, Sarawak, 94300 Malaysia*

[c] *Core Research Facilities, King Fahd University of Petroleum & Minerals, Dhahran, 31261 Saudi Arabia*

**e-mail: mssnasrin@unimas.my*

***e-mail: chzuhairi@usm.my*

Received May 16, 2025; revised July 18, 2025; accepted July 28, 2025

Abstract—The expansion of the oleochemical industry results in excess glycerol production to the extent it is regarded as a waste. This drives the exploration of value-added products like acrylic acid to address the surplus and associated environmental issues. However, current processes mainly focus on the gaseous phase, requiring high temperatures and complex setups. Although some research delves into liquid-phase glycerol oxydehydration, information remains limited. In this study, SBA-15 supported heteropoly phosphotungstic acid (HPW) catalysts (PW/SBA-15) with varied acid loadings (10–40 wt %) were synthesized for a single-step liquid-phase glycerol oxydehydration. The impact of calcination temperatures (400–700°C) on catalyst properties and activity was explored. Extensive characterization techniques were employed to assess surface, morphological, and structural properties. Optimal conditions were identified: 3 h reaction time, 240°C reaction temperature, and 10 wt % catalyst loading, achieving 98.7% glycerol conversion and 22.5% acrylic acid yield. Glycerol oxydehydration followed a pseudo second-order kinetic model with an activation energy of 134.4 kJ/mol. The 30PW/SBA-15 catalyst exhibited a defined structure, effectively catalyzing glycerol-to-acrylic acid oxydehydration due to strong acid sites and appropriate redox sites.

Keywords: liquid phase, oxydehydration, acrylic acid, SBA-15 supported HPW catalysts, mechanism, kinetic study

DOI: 10.1134/S0023158425600713

INTRODUCTION

The global acrylic acid market is projected to witness substantial growth, with its volume expected to surge from approximately 8.12 million metric tons in 2022 to around 11.9 million metric tons by 2030 [1]. Attaining a spot among the top 100 chemicals manufactured worldwide, acrylic acid is recognized as a fundamental compound used in the production of plastics and polymers used in a variety of applications such as adhesives, electronic manufacturing procedures, finishing, inks, leather, sealants, surface coatings, paint, paper treatment, polymer enhancements, and textiles manufacturing [2]. Acrylic acid also exhibits the ability to undergo oxidative polymerization, due to the presence of a highly reactive α–β unsaturated carboxyl group within its molecular structure. This unique property leads to the formation of various downstream polymeric derivatives, which find valuable applications in a wide range of industries. These applications include super adsorbents, fabric components, detergents, paper additives, coating materials, plastics, and more, making acrylic acid a versatile and essential compound for numerous industrial processes [3].

The petrochemical sector presently manufactures over 3 million tons of acrylic acid annually through a dual-step gas-phase oxidation of propane or propylene [4–6]. The production of acrylic acid using propane or propylene as the raw materials faces substantial challenges, including concerns about air and groundwater pollution associated with the use of non-renewable fossil fuels [6]. As a result, it is critical to investigate a new and novel technique for producing acrylic acid that reduces reliance on fossil fuels as soon as possible. As a result, current research works have been shifting

towards employing an oxydehydration reaction for the conversion of glycerol selectively into acrylic acid.

Various catalytic systems were tested for a single-step glycerol oxydehydration reaction including vanadyl pyrophosphate catalysts [7–9], mixed metal oxide catalysts [10–16], molecular sieves supported metal-based catalysts [17–20] and supported heteropoly acid catalysts [21–23]. Heteropoly acids (HPAs) have attracted the interest of scientists due to their application in a multitude of acid-catalyzed processes, setting them apart from other acid catalysts. Their distinguishing trait lies in their strong yet adjustable acidity, facilitating their efficacy in catalyzing a diverse range of organic reactions. Early studies were conducted by Thanasilp et al. [23] where they utilized an impregnation method to synthesize catalysts containing HPAs supported on alumina (HPA/Al_2O_3). These catalysts were subsequently employed in a batch process operated at a temperature as low as 90°C for selective catalysis of the oxydehydration of glycerol in liquid phase. SiW/SBA-15 catalyst showed the best catalytic activity, yielding acrylic acid as high as 25% at about 84% glycerol conversion. In addition to acrylic acid, by-products including glycolic acid and acetic acid, which were produced with yields of approximately 15 and 19%, resulted from an undesired pathway intermediated by acetaldehyde, was also produced. These findings indicate that achieving high yields of acrylic acid in this reaction requires a combination of moderate acid strength and a strong oxidative capability. It is worth noting that this research group utilized a 20 wt % aqueous glycerol solution with a fixed mole ratio of glycerol to H_2O_2 of 1 : 2.

In continuity with their prior work, Thanasilp et al. [22] proceeded to synthesize SiW/HZSM-5 catalysts incorporating metals like Ce, Co, Ni, and V and subsequently evaluated their performance in direct acrylic acid synthesis via oxydehydration of glycerol (20 wt %). Surprisingly, the addition of 6% V to SiW/HZSM-5 improved the process, achieving 32.4% acrylic acid yield at a glycerol conversion of 98.6%. As a result, it can be deduced that V plays a critical role in improving the catalyst's oxidative capabilities while keeping the catalyst's maximal acid strength, which is predominantly due to Brønsted acid sites and is highly required for initiating this oxydehydration reaction. This work also emphasizes the need for optimizing the acidity, oxidative potential, and pore characteristics of the catalyst for future process improvements. Besides, they also performed a kinetic study using V–SiW/HZSM-5 catalysts within a temperature range of 60 to 90°C, and the researchers observed that the reaction rate exhibited a positive correlation with increasing glycerol concentration. The activation energy (E_a) was reported to be 28.57 kJ/mol.

Later, another research group synthesized and employed a range of catalysts, consisting of $Mo_3VO_x/H_4SiW_{12}O_{40}/Al_2O_3$, to facilitate the single-step oxydehydration of 20 wt % glycerol to yield acrylic acid [21]. The researchers discovered that altering the Mo_3VO_x content in catalysts resulted in similar acetic acid and acrylic acid yields. Above 550°C, increasing the temperature of calcination from 350 to 650°C caused structural changes in the catalyst, including increased crystallinity of Mo_3VO_x and the formation of $(V/Mo)O_x$ compounds. At approximately 450°C, diverse WO_x species formed as a result of the dissociation of the $H_4SiW_{12}O_{40}$ Keggin structure. At temperatures exceeding 450°C, acrylic acid yield declined, accompanied by an increase in acrolein yield, while the production of acetic acid remained essentially unaffected.

It should be noted that in all three studies, the initial glycerol concentration used was only 20 wt %, which resulted in high yield percentages in all cases. However, despite these high percentages, the actual production of acrylic acid remained relatively low [24]. Hence, enhancing bifunctional catalysts in the single-step glycerol-to-acrylic acid conversion requires fine tuning of both acidic and redox properties. Also, there is a lack of information and in depth analysis regarding the kinetic study of glycerol oxydehydration reactions.-Building on our previous research [25], this study aims to deepen understanding of the catalytic behavior of SBA-15-supported heteropoly phosphotungstic acid (HPW), PW/SBA-15, by elucidating the reaction mechanism and performing a comprehensive kinetic analysis.

EXPERIMENTAL

Catalyst Synthesis

The SBA-15 support was prepared following a published method [26]. In this study, PW/SBA-15 catalysts with different acid loadings (10, 20, 30, and 40 wt %) were synthesized. The incorporation of HPW via incipient wetness impregnation was carried out by varying the amount of $H_3PW_{12}O_{40} \cdot H_2O$ according to the respective acid loadings. The mixture was continuously stirred at 200 rpm at an ambient temperature for 3 h. After drying at 110°C for 20 h, the supported catalysts were calcined at 400°C for 4 h. The resulting catalysts are designated as *x*PW/SBA-15 in which *x* stands for the weight percent of HPW in SBA-15. Subsequently, PW/SBA-15 catalysts with the best acid loading determined from the previous catalytic tests (i.e., 30 wt %) synthesized by varying the calcination temperature. The catalysts were calcined at 400, 500, 600, or 700°C for 4 h, with a heating rate of 2°C per min. The resulting catalysts are labeled as PW/SBA-15(*y*), where *y* indicates the calcination temperature (°C).

Catalyst Characterization

The surface and pore characteristics of the synthesized catalysts were analyzed using nitrogen adsorp-

tion–desorption measurements with a Micromeritics ASAP 2020 instrument. Prior to analysis, the powder samples were degassed at 200°C for 4 h under vacuum ($P < 10^{-1}$ Pa) to remove adsorbed impurities. The Brunauer–Emmett–Teller (BET) method and Barrett–Joyner–Halenda (BJH) model were employed to ascertain specific surface area and pore size. The calculation of the total pore volume involved measuring nitrogen adsorption at a relative pressure (P/P_0) of 0.98. Next, a Quanta FEG 450 scanning electron microscopy (SEM) equipment was utilized to characterize the surface morphological changes with varying acid loadings and calcination temperatures. Meanwhile, transmission electron microscopy (TEM) was used to verify the hexagonal arrays and straight pores in SBA-15 and to examine the catalyst structures with varying acid loadings. The images were captured with a Philips FEI CM 12 TEM instrument at 120 kV. Fourier-transform infrared (FTIR) spectroscopy analysis was conducted to investigate the chemical bonds between SBA-15 and catalysts. Samples were prepared using the KBr pellet technique with 0.9 mg of the sample and 63 mg of KBr, pressed into pellets. Spectra were recorded in the range of 4000–400 cm^{-1} using a Perkin-Elmer 2000 system. Finally, acid properties of the catalysts were evaluated using temperature programmed desorption of NH_3 (NH_3-TPD) on a Micromeritics AutoChem II 2920 instrument with a thermal conductivity detector (TCD). A 0.05 g sample was pretreated in He at 200°C for 60 min, followed by NH_3 adsorption at 120°C. Subsequently, NH_3 desorption was carried out by heating the sample from 120 to 700°C at a rate of 10°C/min.

Reaction Procedure and Product Analysis

The glycerol oxydehydration reaction to produce acrylic acid was carried out in a batch reactor setup. In a typical experiment, 15 g of 85% glycerol stock was mixed with the specified amount of catalyst (e.g., 10 wt % of PW/SBA-15 with respect to glycerol) in a 100 mL stainless-steel gasket reactor equipped with a magnetic stirring bar. The reactor was properly tightened to maintain a close system. Prior to the reaction, the reactor was purged with O_2 for 10 min to remove air and create an O_2-rich atmosphere. The temperature controller was then used to set the target temperature to 230°C, and the mixture was stirred continuously at 300 rpm for 5 h. Following this period, the reaction was quenched by rapidly cooling the reactor in an ice bath. The experiment was repeated using different acid loadings. Next, to study the effect of operating conditions, 15 g of glycerol was mixed with the desired amount of the best catalyst and tested for different reaction times (1–7 h). After achieving the best reaction time, the reaction was carried out to investigate the effect of various reaction temperatures (210–240°C) and catalyst loading (6–12 wt %).

After the reaction, the reactor was cooled and the liquid product was centrifuged at 4400 rpm for 40 min to separate the catalyst. Following the reaction, 2 mL of the liquid mixture was filtered through a 0.22 μm PTFE syringe filter. For analysis, a 100 μL aliquot of the filtered sample was diluted 1:100 in an aqueous pH 2.0 H_3PO_4 solution. Quantitative analysis was performed on an Agilent 1260 Infinity HPLC system equipped with a ZORBAX Eclipse Plus C18 column (4.6 × 100 mm, 3.5 μm) and a refractive index detector (RID). The injection volume was 5 μL, with the column and RID temperatures maintained at 40 and 35°C, respectively. The mobile phase, 0.001 M H_3PO_4 (pH 2.0), was eluted at a flow rate of 0.5 mL/min. Glycerol conversion (X), product yield (Y), and selectivity (S) were calculated according to the equations adapted from Shen et al. [27]:

$$X = \left(\frac{n_{\text{Gly, initial}} - n_{\text{Gly,final}}}{n_{\text{Gly, initial}}}\right) \times 100\%, \quad (1)$$

$$Y = \left(\frac{n_{\text{AA}}}{n_{\text{Gly,initial}}}\right) \times 100\%, \quad (2)$$

$$S = \left(\frac{Y}{X}\right) \times 100\%, \quad (3)$$

where $n_{\text{Gly,initial}}$ is the initial concentration of glycerol (M); $n_{\text{Gly,final}}$ is the final concentration of glycerol (M); n_{AA} is the concentration of acrylic acid (M).

Additionally, a gas chromatography–mass spectrometry (GC–MS) analysis was conducted to identify all generated products under the best reaction conditions. The analysis was carried out using an Agilent GC 7890A/MS 5975 instrument, equipped with a DBwax capillary column. From the GC–MS chromatogram, a plausible mechanism for glycerol oxydehydration reaction was proposed.

The kinetics of glycerol oxydehydration to acrylic acid was studied using the most potential catalyst. The experiment involved varying the reaction temperature from 210 to 240°C under the optimal reaction condition (i.e., 10 wt % catalyst loading relative to glycerol). Kinetic parameters such as reaction rate constant (k), activation energy (E_a), and pre-exponential factor (A) were determined. A kinetic model for the glycerol-to-acrylic acid oxydehydration reaction was then proposed. Equation (4) was used to calculate the reaction rate constant (k), with several assumptions made during the derivation of the rate equation: (i). the reaction consists of parallel and consecutive reactions; thus, a second-order reaction is assumed; (ii) the reaction is considered irreversible and (iii) the reaction is conducted in an isothermal batch reactor. Thus, by integrating mole balance, rate law, and reaction stoichiometry, the rate expression is derived as follows:

$$\frac{dX}{dt} = k[C_{\text{Gly, initial}}(1 - X)]^2. \quad (4)$$

Table 1. Textural and chemical properties of PW/SBA-15 catalysts

Catalyst	Total surface area, m^2/g	External surface area, m^2/g	Micropore area, m^2/g	Total pore volume, cm^3/g	Average pore size, Å	Acid amount, mmol NH_3/g_{cat}	Total acidity, mmol NH_3/g_{cat}
SBA-15	737	448	289	0.6275	52.06	NA	NA
10PW/SBA-15	538	381	157	0.5452	52.41	0.293 (89°C) 0.149 (530°C)	0.442
20PW/SBA-15	447	310	136	0.4435	54.89	0.424 (124°C) 0.099 (530°C)	0.523
30PW/SBA-15	418	298	120	0.4437	53.64	0.412 (91°C) 0.129 (326°C) 0.105 (535°C)	0.707
40PW/SBA-15	382	278	104	0.3994	56.21	0.408 (98°C) 0.056 (332°C) 0.019 (535°C)	0.483
30PW/SBA-15(400)	418	298	120	0.4437	53.64	NA	NA
30PW/SBA-15(500)	447	320	127	0.4876	55.48	NA	NA
30PW/SBA-15(600)	326	227	98	0.3248	55.17	NA	NA
30PW/SBA-15(700)	292	222	71	0.3650	54.25	NA	NA

NA means not available

Here k is the rate constant ($M^{-1}\ h^{-1}$); $C_{Gly,initial}$ is the initial concentration of glycerol (mol/L); X is the glycerol conversion.

This equation was solved using MATLAB's ODE solver (ode45 function), followed by the f*minsearch* function to calculate the corresponding k values at different reaction temperatures (210–240°C) [28]. Using the Arrhenius equation, the values of A and E_a were obtained from a linear plot of $\ln(k)$ *vs.* $1/T$:

$$k = Ae^{-E_a/RT}. \quad (5)$$

Here A is the pre-exponential factor; E_a is the activation energy (J/mol); R is the universal gas constant (8.3142 J $mol^{-1}\ K^{-1}$); T is the temperature (K).

Furthermore, a kinetic model for the conversion of glycerol to acrylic acid via oxydehydration is presented, and its accuracy in predicting glycerol conversion is validated using the sum of squared errors (SSE) calculated in MATLAB software. Generally, SSE quantifies the differences between the simulated and experimental data and is expressed as:

$$\mathrm{SSE} = \sum_{i=0}^{N} \left(x_i - \overline{x}_i(k)\right)^2, \quad (6)$$

where N is the total number of data points; x is actual data in the experiment; $\overline{x}$ is simulated data from the model.

RESULTS AND DISCUSSION

Influence of Different Acid Loadings

Using N_2 physisorption analysis, the textural properties of the prepared PW/SBA-15 catalysts with varying acid loadings were investigated and the results are shown in Table 1. With increasing HPW loading, the total surface area and total pore volume of the catalyst marginally dropped from 538 to 382 m^2/g and from 0.5452 to 0.3994 cm^3/g, respectively. The primary reason for the decrease might be related to the formation of bulk HPW crystals in the SBA-15 support pores. The decreasing trends in surface area and pore volume are in line with previous reports [29, 30].

Furthermore, the average pore sizes of all synthesized catalysts closely resemble those of the SBA-15 support, specifically falling within the range of 52–56 Å. This demonstrates that all supported catalysts could maintain mesoporous structures after HPA incorporation. However, there are slight increases in the average pore size at higher HPW loadings (40 wt %) compared to SBA-15 support. One potential explanation for this phenomenon could be the increased formation of tungsten trioxide on the surface of the SBA-15 support at higher loadings, resulting in the creation of secondary pores. These secondary pores likely contributed to the observed rise in the average pore size, as illustrated in Table 1. Comparable observations were also documented by Hoo and Abdullah [31] under identical acid loading conditions.

Figure 1 depicts the SEM (Figs. 1a–1e) and TEM (Figs. 1f–1j) images acquired for all synthesized cata-

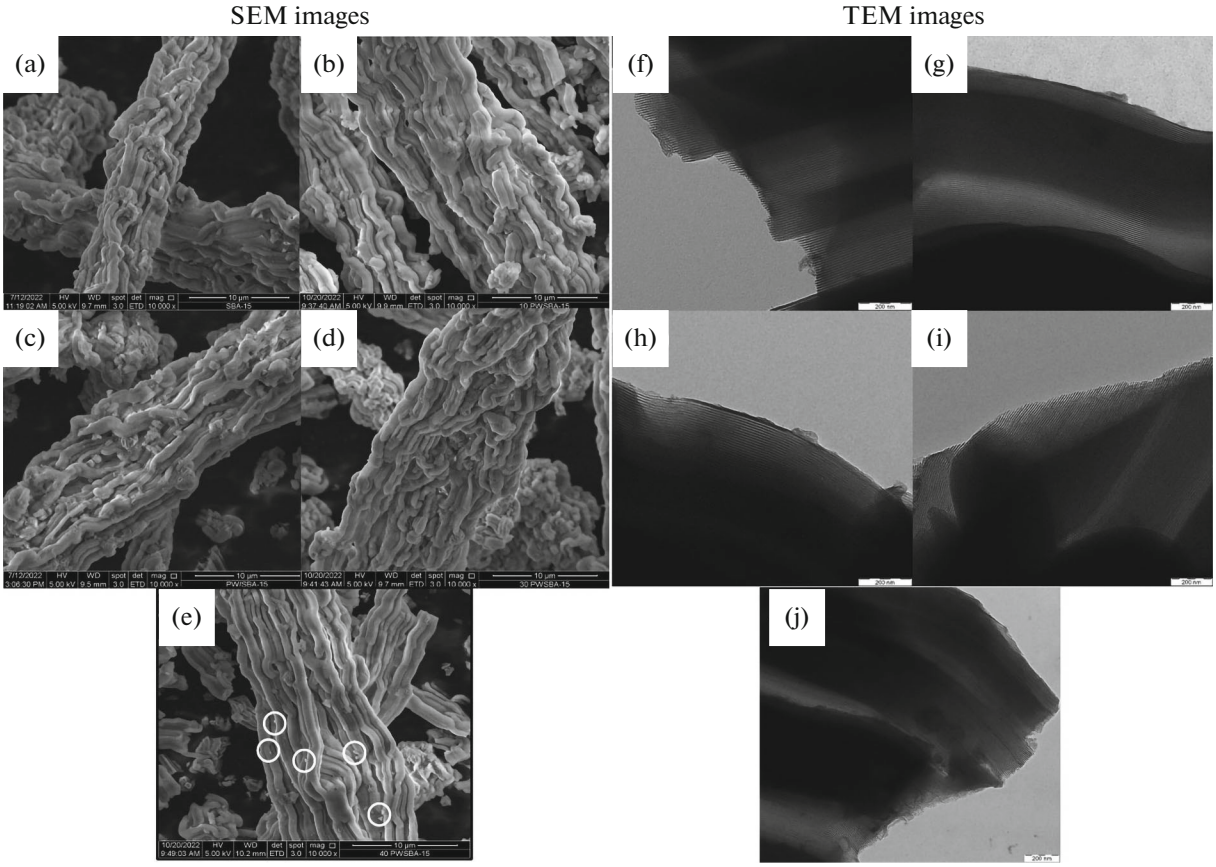

Fig. 1. SEM images at a magnification of 10000X (a–e) and TEM images at a magnification of 40000X (f–j) of SBA-15 (a, f), 10PW/SBA-15 (b, g), 20PW/SBA-15 (c, h), 30PW/SBA-15 (d, i), and 40PW/SBA-15 (e, j) catalysts.

lysts. Overall, all catalysts exhibited the characteristic morphology of SBA-15, featuring an elongated rod-like shape with a mesoporous structure, consistent with prior reports [32]. This result confirms the successful synthesis of all catalysts, as the elongated fibrous mesoporous channels remained intact even at HPW loadings up to 40 wt %.

However, catalysts with higher loading (i.e., 40PW/SBA-15) display visible HPW crystals on their external surface. Increasing the catalyst loading led to the saturation of the internal mesopores, which were partially narrowed, resulting in the deposition of the active material on the external surface [26]. The excess of HPW that could not be accommodated within the mesopores was then deposited on the external surface and observed as visible crystals. Interestingly, unlike in other reported study [31], the PW/SBA-15 catalysts synthesized in this study showed the absence of any visible microcrystals populating the external surface of SBA-15, even at a high loading of 30 wt %. This observation provided strong evidence that the active material was well dispersed within the internal mesopores of the support, indicating rather uniform dispersions.

Figures 1f–1j show that, similar to SBA-15, all catalysts exhibited highly ordered mesoporous channels [33]. These results indicate the successful creation of well-ordered mesopores, even at HPW loadings as high as 40 wt %. Additionally, Figs. 1f–1j illustrates that the impregnation of HPW anions did not induce substantial structural alterations in SBA-15, as evidenced by the absence of significant internal mesopore distortion. These findings indicate that SBA-15's uniform structure was preserved despite the introduction of HPW anions. Additionally, they suggest that HPW species were effectively dispersed within the hexagonal channels, confirming the earlier surface analysis results. Frattini et al. [34] reported similar observations where the ordered structure of mesoporous SBA-15 support was still preserved even at higher HPW loadings up to 55.7 wt %.

Figure 2a shows the FTIR spectra of all synthesized catalysts and SBA-15, covering the range from 1400 to 400 cm^{-1}. As depicted, the broad band corresponding to the Si–O–Si asymmetric stretching, a characteristic feature of SBA-15, was observed in the range of 1220–1064 cm^{-1}. Besides, SBA-15 support also exhibited two distinct bands at 800 and 462 cm^{-1}, corresponding to the Si–O–Si symmetric stretching band and the bending vibrational mode of Si–O–Si, respectively [35]. This may be due to Si–OH surface

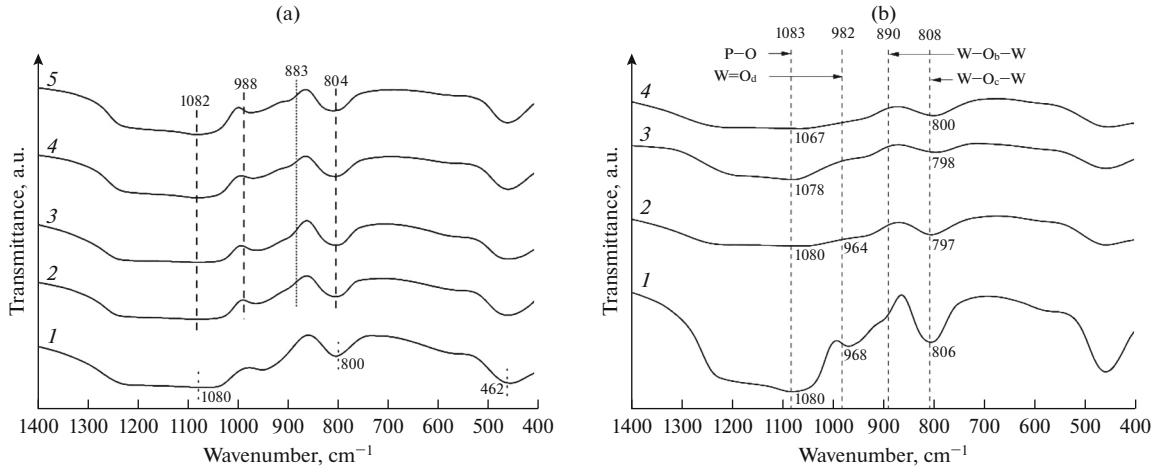

Fig. 2. (a) FTIR spectra of SBA-15 (*1*), 10PW/SBA-15 (*2*), 20PW/SBA-15 (*3*), 30PW/SBA-15 (*4*), and 40PW/SBA-15 (*5*) catalysts. (b) FTIR spectra of 30PW/SBA-15(400) (*1*), 30PW/SBA-15(500) (*2*), 30PW/SBA-15(600) (*3*), and 30PW/SBA-15(700) (*4*) catalysts.

absorption, which results in hydrogen bond formation [36]. Interestingly, the vibration bands at 1080, 800, and 462 cm^{-1} are found consistently in all synthesized catalysts. This indicates that, despite HPW incorporation at all loadings, the SBA-15 support preserved its desirable silica framework.

The spectra also exhibit characteristic bands of HPW Keggin ions [37]. Specifically, the symmetric P–O stretch of the central tetrahedron at 1082 cm^{-1} was observed in all supported catalysts (Fig. 2a). Notably, a red shift is apparent in the W=O$_d$ band for all synthesized catalysts compared to the original pure HPW band (988 cm^{-1}). The W=O$_d$ stretching bands shifted to lower wavenumbers with decreasing HPW loading: 974 cm^{-1} for 40PW/SBA-15, 968 cm^{-1} for 30PW/SBA-15, 964 cm^{-1} for 20PW/SBA-15, and 962 cm^{-1} for 10PW/SBA-15.

The observed phenomenon can be ascribed to the interaction of HPW anions with the SBA-15 support [38]. The shift observed in W=O$_d$ bands points to a clear interaction between Keggin anions and support, suggesting that the W=O$_d$ bonds within HPW anions serve as strong electron donors [39]. Additionally, none of the four supported catalysts exhibited the W–O$_b$–W band, which was supposed to be at 883 cm^{-1}. This observation could be attributed to the potential masking effect resulting from other highly intense bands, particularly those in the range of 850–900 cm^{-1}. Furthermore, the characteristic vibrations associated with edge-shared oxygen (W–O$_c$–W) at 804 cm^{-1} were detected in all synthesized catalysts. The presence of those bands indicates that the intricate structure of the HPW Keggin ion incorporated into the support was preserved and significant molecular changes were expected.

Using NH_3-TPD, the acid properties of the SBA-15 supported HPW catalysts, including acidic site amount and acid strength were characterized and the profiles of the four samples are depicted in Fig. 3. In general, acid sites can be categorized based on their strength, which includes weak- (150–300°C), medium- (300–500°C) and strong- (500–650°C) acidity levels [37]. One broad NH_3-TPD peak and one hump were observed at 89 and 530°C, respectively for the 10PW/SBA-15 catalyst indicating that both weak- and strong-strength acid sites are present in its structure. The 20PW/SBA-15 catalyst demonstrated a comparable outcome, showing both weak- and strong-strength acid sites. This was evident from the observation of a single broad peak and a hump during the analysis, occurring at temperatures of 124 and 530°C, respectively. As HPW loading was increased, it was found that the 30PW/SBA-15 and 40PW/SBA-15 catalysts displayed similar trends in the NH_3 desorption profiles. NH_3 profiles exhibited one broad peak and two humps for 30PW/SBA-15 and 40PW/SBA-15 catalysts, centered at around 91, 326, 535 and 98, 332, 535°C, respectively, indicating the presence of weak, medium, and strong acid sites in both catalyst structures.

Table 1 summarizes the quantitative analysis of acid sites from NH_3-TPD for all supported catalysts. The total acidity of the PW/SBA-15 catalysts decreased in the following order: 30PW/SBA-15 > 20PW/SBA-15 > 40PW/SBA-15 > 10PW/SBA-15. Generally, catalyst acidity increases with higher HPA loading. Nevertheless, in this scenario, the increase in HPW content did not result in a corresponding increase in acid site concentration. This suggests that not all HPW acid sites were accessible for NH_3 adsorption. This is presumably due to the agglomeration of

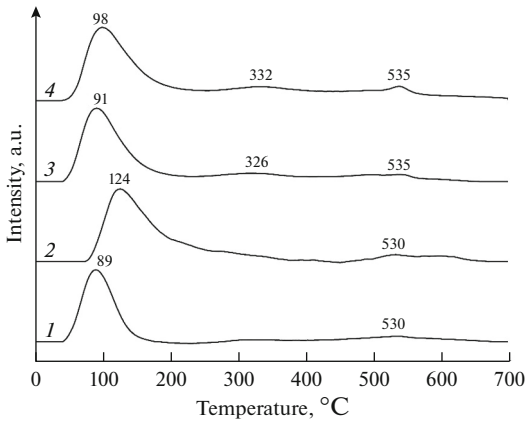

Fig. 3. NH_3-TPD profiles of 10PW/SBA-15 (*1*), 20PW/SBA-15 (*2*), 30PW/SBA-15 (*3*), and 40PW/SBA-15 (*4*) catalysts.

HPW during the impregnation process into SBA-15 supports.

The decrease in acidity of the 40PW/SBA-15 catalyst can be attributed to two factors: partial pore blockage at high HPW loading and the reduction in HPW acidity due to the oxidation of HPW anions. This oxidation led to the formation of WO_3, which lacked acidic properties [31].

The performance of the PW/SBA-15 catalysts with various acid loadings was investigated for glycerol oxydehydration in the liquid phase. The reaction was carried out for 5 h at 230°C using 15 g of 85% stock glycerol as the reactant and a catalyst loading from 10 to 40 wt %. (Fig. 4). Increasing the HPW loading from 10 to 30 wt % led to a substantial increase in glycerol conversion, rising from 29.7 to 87.8%. The well-dispersed HPW on SBA-15 improved accessibility of glycerol molecules to the catalytically active protons present on the supported catalyst, thereby increasing the glycerol conversion [40]. However, 40PW/SBA-15 showed the highest glycerol conversion (94.1%), although its total acidity is lower than that of 20PW/SBA-15 and 30PW/SBA-15. This phenomenon may be attributed to the presence of more active material on the SBA-15 catalyst's surface rather than within its mesopores. This abundance of active material on the surface could lead to glycerol side reactions, which contributed to higher glycerol conversion.

It's worth mentioning that all four catalysts effectively catalyzed the single-step conversion of glycerol to acrylic acid through oxydehydration. The catalytic activity of PW/SBA-15 with various acid loadings decreased in the order: 30PW/SBA-15 (17.5%) > 20PW/SBA-15 (15.9%) > 40PW/SBA-15 (11.0%) > 10PW/SBA-15 (0.7%) consistent with their acid

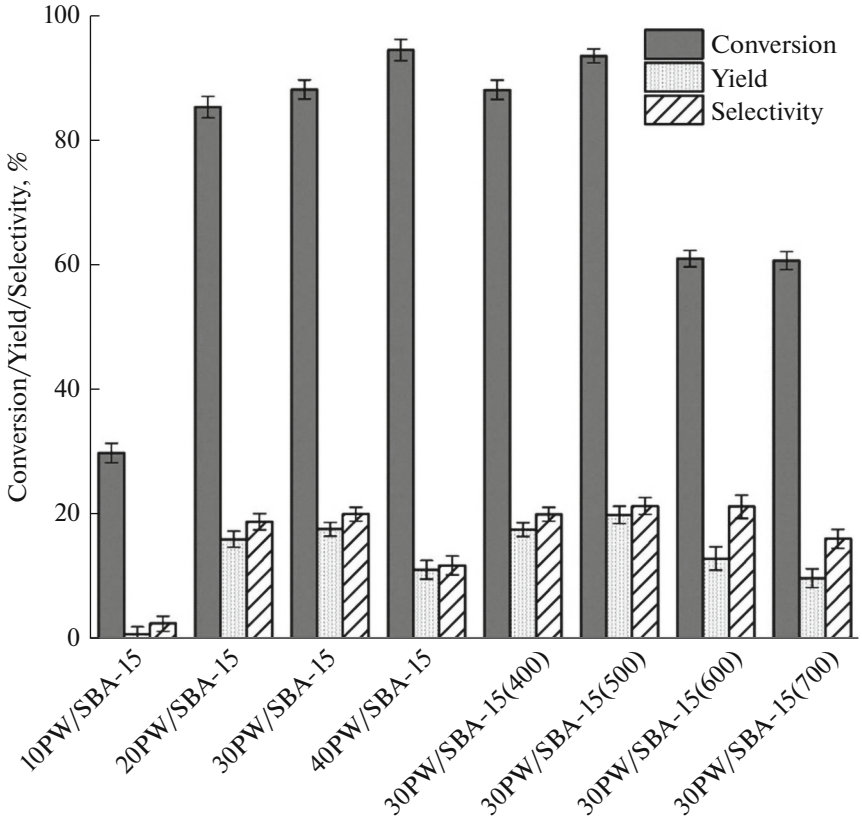

Fig. 4. Performance of PW/SBA-15 in glycerol oxydehydration to acrylic acid.

strength. In theory, enhancing a catalyst's acidity should result in higher catalytic activity [41]. Given the low loading of HPW anions, it is reasonable to expect that the 10PW/SBA-15 catalyst would exhibit lower reactivity compared to other solid catalysts. This might be ascribed to the poor presence of active sites resulting from the low amount of HPW loaded onto the catalyst. However, despite a higher HPW anion loadings, the 40PW/SBA-15 catalyst demonstrated reduced activity compared with 20PW/SBA-15 and 30PW/SBA-15, suggesting that at HPW loadings exceeding 30 wt %, the mesopores may have experienced significant blockages. Consequently, the acid sites within these mesopores may have been inaccessible during the reaction [42].

Influence of Calcination Temperature

The temperature at which the catalyst is calcined plays a crucial role in synthesizing catalysts, since it considerably affects their physical and chemical properties [21]. The textural properties of 30PW/SBA-15 catalysts with different calcination temperatures were investigated using N_2 adsorption–desorption analysis, and the results are presented in Table 1. Increasing the calcination temperature from 400 to 500°C increased the BET surface area from 418 to 447 m^2/g and the total pore volume from 0.4437 to 0.4876 cm^3/g, due to the elimination of organic matter [43]. However, the surface area and total pore volume decreased from 447 to 292 m^2/g and from 0.4876 to 0.3650 cm^3/g, respectively, as the temperature was increased from 500 to 700°C. The subsequent decline in the surface area and total pore volume upon thermal treatment at higher temperatures could be due to the collapse of pores and increase in particle size of the catalysts.

Furthermore, the average pore size increased slightly from 53.64 to 54.25 Å as the temperature rose from 400 to 700°C. This observation, consistent with the findings of Chen et al. [44], is attributed to the partial collapse of the porous structure at higher calcination temperatures. Notably, this value remains comparable to that of the as-prepared SBA-15 support (52.06 Å), demonstrating that the mesoporous structure was largely preserved after thermal treatment. Overall, elevating the calcination temperature from 400 to 700°C reduced the surface area and pore volume but slightly increased the average pore diameter.

Figure 2b presents detailed FTIR spectra for all synthesized catalysts calcined at different temperatures, covering the range from 1400 to 400 cm^{-1}. The spectra exhibit characteristic bands of the HPW Keggin anion, including the asymmetric P–O stretching at the central tetrahedron (1083 cm^{-1}), terminal asymmetric oxygen ($W=O_d$) at 982 cm^{-1}, corner-shared asymmetric oxygen ($W-O_b-W$) at 890 cm^{-1}, and typical vibrations of edge-shared oxygen ($W-O_c-W$) at 804 cm^{-1}, as summarized for comparison [45]. One of the most interesting observations from the FTIR spectra shown in Fig. 2b was the decrease in wavenumber (red shift) of the P–O band which could be detected in all supported catalysts. The higher the calcination temperature, the further the P–O band shifts. Such observations suggested the possibility of changes in the Keggin unit structure due to the high calcination temperature.

Furthermore, the PW/SBA-15(400) and PW/SBA-15(500) catalysts exhibited a red shift of the $W=O_d$ band which can serve as the indication of the interaction between HPW anions and the SBA-15 support [39]. HPW anions are polyoxoanions that are rich in electrons, making them strong acid sites because of their ability to donate electrons via terminal $W=O_d$ bonds. The observation of a red shift in the $W=O_d$ band indicates an interaction between the Keggin HPW anions and the support material. This interaction leads to the support material exhibiting strong electron-donating properties, which can be attributed to the presence of the $W=O_d$ group [39]. However, as the reaction temperature increased from 500 to 700°C, a reduction in the $W=O_d$ band intensity was observed. This loss in intensity suggests a symmetrical breakdown within the Keggin unit, likely due to partial structural collapse during the calcination at higher temperatures [46].

The $W-O_b-W$ band at 890 cm^{-1} was barely detected in all synthesized catalysts, likely due to masking by intense bands between 850 and 900 cm^{-1}. Similarly, the $W-O_c-W$ band at 808 cm^{-1} overlapped with the strong symmetric stretching and bending vibrations of the Si–O–Si band in SBA-15 at 804 cm^{-1}. These observations, along with the interactions between HPW anions and the SBA-15 support at calcination temperatures of 400 and 500°C, indicate successful HPW impregnation. However, increasing the calcination temperature to 700°C altered the HPW Keggin structure, potentially impacting catalytic performance.

Figure 4 shows that the catalyst's calcination temperature significantly influences glycerol oxydehydration. The PW/SBA-15(500) catalyst exhibited the highest activity, achieving 93.2% glycerol conversion and 20.0% acrylic acid yield. Its large surface area and total pore volume provide numerous strong acidic sites uniformly distributed on the surface. Additionally, the catalyst's large average pore diameter (55.48 Å) reduces pore diffusion limitations, enhancing acrylic acid selectivity. In comparison, the PW/SBA-15(400) catalyst showed slightly lower activity, likely due to its smaller surface area, which limits glycerol interaction with strong acid sites.

Increasing the calcination temperature from 500 to 700°C led to a decline in catalyst activity, with glycerol conversion dropping from 93.2 to 60.5%. This decrease is attributed to reduced catalyst acidity

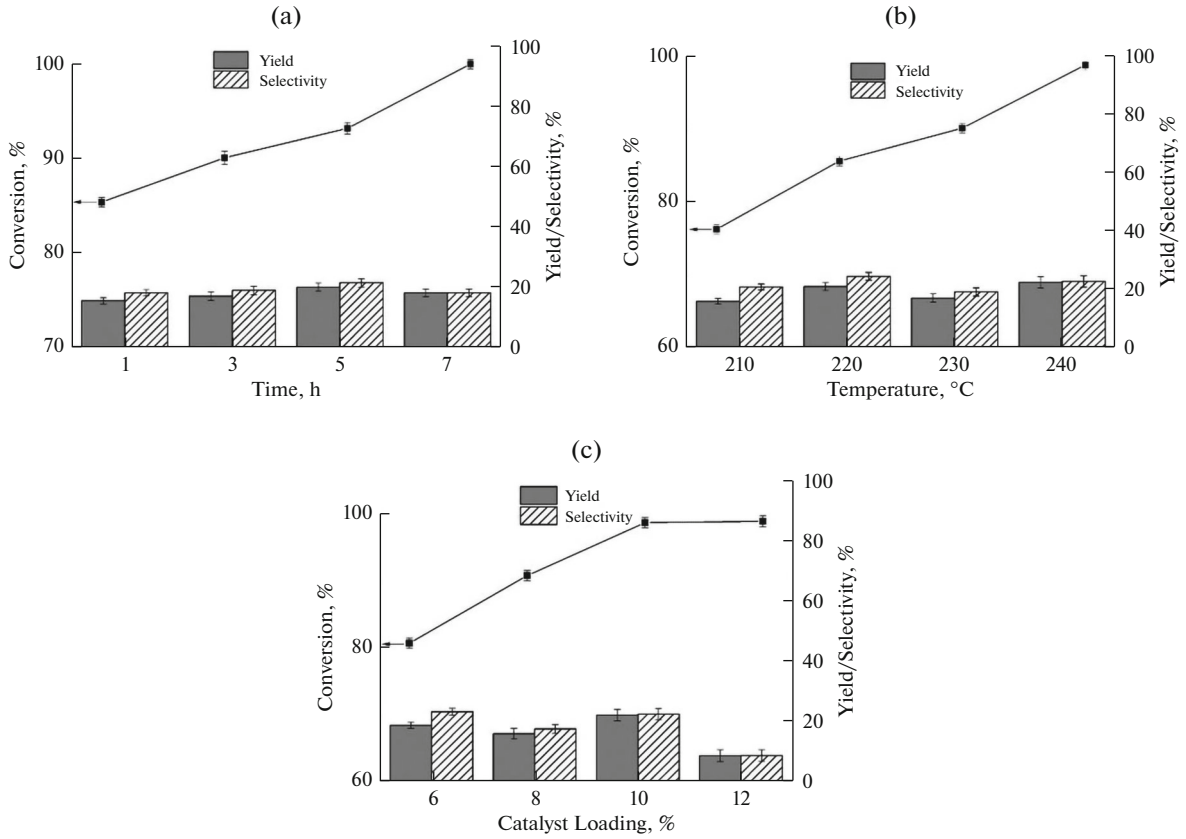

Fig. 5. The influence of reaction time (a), reaction temperature (b), and catalyst loading (c) on the catalytic performance of 30PW/SBA-15(500) catalyst in glycerol oxydehydration to acrylic acid.

caused by the thermal degradation of HPW Keggin units into P_2O_5 and WO_3 at higher temperatures [46, 47]. This observation aligns with the FTIR analysis, which revealed a loss in the $W{=}O_d$ band when the temperature was raised from 500 to 700°C. Another research group [21] also reported a similar finding, where the conversion of glycerol and corresponding acrylic acid selectivity experienced significant drops upon subjecting the catalyst to elevated calcination temperatures of 550 and 650°C. Therefore, it can be concluded that the catalyst's activity experienced a substantial decline as the calcination temperature increased. In this case, the observed phenomenon is attributable to the decreasing catalyst acidity that is caused by the decomposition of the HPW Keggin unit, which reduces the acidity of the catalyst. In this study, PW/SBA-15 catalysts with 30 wt % acid loading calcined at 500°C showed the highest activity. Therefore, the 30PW/SBA-15(500) catalyst was selected to examine the influence of operating conditions on glycerol oxydehydration to acrylic acid.

Influence of Reaction Time

The effects of reaction time on the conversion of glycerol and acrylic acid yield were investigated by varying the reaction time (1–7 h). The reaction was carried out at 230°C by using 15 g of 85% stock glycerol as the reactant and a catalyst loading of 10 wt %. Figure 5a shows the catalytic activity in glycerol oxydehydration to yield acrylic acid at various reaction times.

The results showed that increasing the reaction time improved glycerol conversion. In particular, with the extension of the reaction time from 1 to 7 h, glycerol conversion increased from 85.4 to 100%. The increase in conversion can be ascribed to the improved interaction between reactant molecules and active sites as the reaction progressed over an extended period, leading to the generation of acrylic acid and accompanying by-products. However, the slight increase in the conversion suggested that the reaction started to reach equilibrium in which a further increase in reaction time could not improve the conversion.

Furthermore, it can be observed that acrylic acid yield increases with reaction time. The acrylic acid yield saw a notable increase from 15.3 to 20.0% as the reaction time was extended from 1 to 5 h. However, increasing the reaction time to 7 h caused an apparent drop in acrylic acid yield to approximately 17.9% at the same reaction conditions. This observation suggested the formation of other by-products due to further

dehydration and oxidation of glycerol [48, 49]. Although glycerol conversion and acrylic acid yield peaked after 5 h, the increases relative to the 3-hour reaction were marginal—only 3.1 and 1.9%, respectively. Hence, it was not worthwhile to further prolong the reaction by an extra two hours to achieve only minimal improvement in conversion and yield. A reaction time of 3 h was sufficient to minimize undesired by-product formation while keeping the process time efficient.

Influence of Reaction Temperature

In this study, the reaction temperature was varied from 220 to 240°C, while employing 15 g of 85% stock glycerol as the reactant and a catalyst loading of 10 wt %. Figure 5b clearly demonstrates that glycerol conversion increases with temperature, consistent with previous studies [7, 15]. Considering that glycerol dehydration is an endothermic reaction, the increase in reaction temperature would substantially influence glycerol conversion. For instance, at a reaction time of 3 h, the conversion of glycerol was 76.2% at 210°C, whereas at 220, 230 and 240°C, the conversions were 85.6, 90.1, and 98.7%, respectively. Low conversion was observed at 210°C due to the low kinetic energy which slowed down the activity. However, with the increase in reaction temperature, the kinetic energy correspondingly rose. This observation supports the fact that higher reaction temperatures enhance molecular mobility [50]. At elevated temperatures, molecular velocities tend to be faster, resulting in a higher frequency of collisions between the reactant and catalyst. As a result, this acceleration in the reaction rate caused a notable increase in the reactants' conversion.

Furthermore, an increase in reaction temperature was observed to enhance acrylic acid yield. Specifically, the acrylic acid yield significantly rose from 15.7 to 22.2%, as the reaction temperature was elevated from 210 to 240°C. These results suggest effective interaction between reactant molecules and the catalyst's active sites. Higher temperatures reduced molecular residence time and enhanced mass transfer due to increased kinetic energy. Consequently, reactants efficiently accessed both the inner and outer pores of the 30PW/SBA-15(500) catalyst, which were rich in acid and redox sites. This enhanced accessibility to active sites resulted in an elevated number of active collisions, ultimately leading to a remarkable improvement in catalytic activity [51].

Nevertheless, the acrylic acid yield decreased slightly to 16.8% at 230°C. This observation was in contrast with the consistent trend observed in glycerol conversion, highlighting the non-straightforward correlation in acrylic acid yield and temperature. Due to the weakly endothermic dehydration and strongly exothermic redox reactions, the overall reaction system is thermodynamically self-sustaining [52]. The interplay between these reactions, each responding differently to temperature, is particularly significant in this complex system, which involves both parallel and consecutive reaction pathways.

Concurrently, the rise in acrylic acid yield observed at 240°C resulted from the efficient interplay between the molecules of reactants and the active sites on the surface of the catalyst. Higher temperatures led to a reduced residence time for the molecules, facilitating rapid mass transfer due to the increased kinetic energy. As a result, reactants efficiently accessed both the inner and outer pores of the 30PW/SBA-15(500) catalyst, which contained abundant acid and redox sites. This enhanced accessibility to active sites resulted in an elevated number of active collisions, ultimately leading to a remarkable improvement in catalytic activity [51]. Nevertheless, the acrylic acid yield decreased slightly to 16.8% at 230°C.

These results suggest the formation of side products, such as acetic acid and CO_x, from overoxidation at higher temperatures, which reduced acrylic acid selectivity [53]. The performance of the PW/SBA-15 catalyst at 240°C surpassed that reported by Lopez-Pedrajas et al. [7], who observed less than 5% acrylic acid yield at 30% conversion using an AlVPO catalyst at 250°C. This comparison confirms the superior activity and selectivity of the 30PW/SBA-15(500) catalyst for acrylic acid formation. Consequently, a reaction temperature of 240°C was selected for further investigation due to its optimal catalytic performance, high glycerol conversion, and high acrylic acid yield.

Influence of Catalyst Loading

Figure 5c illustrates the effect of catalyst loading on glycerol oxydehydration to acrylic acid. The reaction was performed at 240°C for 3 h using 15 g of 85% stock glycerol as the reactant, with catalyst loadings ranging from 6 to 12 wt %. Increasing the loading from 6 to 10 wt % led to a significant increase in the glycerol conversion from 80.7 to 98.7%. This notable enhancement can be ascribed to the augmented quantity of active sites on the catalyst surface, facilitating highly efficient interactions with reactant molecules. However, it is noteworthy that further augmenting the catalyst loading to 12 wt % resulted in only a marginal improvement in glycerol conversion to 98.9%, indicating a saturation point beyond which additional catalysts did not contribute to further enhancement in conversion. Interestingly, a similar observation was reported in a prior study [23] by using different HPAs supported on Al_2O_3 catalysts.

Moreover, augmenting the loading of the catalyst from 6 to 10 wt % led to a noteworthy improvement in the acrylic acid yield, rising from 18.8 to 22.2%. This increase was attributed to the augmented quantity of active sites accessible on the catalyst, facilitating a more efficient conversion of glycerol to acrylic acid. However, the yield declined to 8.7% when the catalyst loading was further raised to 12 wt %. It is evident that the glycerol conversion demonstrates a more predictable pattern compared to the acrylic acid yield, which

appears to lack a distinct trend, largely due to the complexity of the reaction. Indeed, at certain catalyst loadings, the formation of intermediates and by-products increased, reducing acrylic acid production. This observation can be attributed to the high catalyst loading, which increased the number of acidic and redox sites, thereby accelerating glycerol oxydehydration and promoting the formation of undesired by-products [23]. Moreover, the decrease in the yield of desired products due to high catalyst loading can be attributed to the reduced mass transfer rate of reactants to the catalyst surface. An increase in catalyst loading could lead to a higher viscosity or density of the reaction mixture, which hinders the movement and diffusion of reactant molecules. As a result, reactants might have difficulty in reaching the catalyst surface efficiently. In summary, the optimal reaction conditions were determined to be a 3-hour reaction time at 240°C with a 10 wt % catalyst loading. Under these conditions, the 30PW/SBA-15(500) catalyst achieved maximum glycerol conversion (98.7%) and a high acrylic acid yield (22.2%).

Reaction Mechanism

The 30PW/SBA-15(500) catalyst was chosen to study the reaction mechanism of glycerol oxydehydration to acrylic acid by varying the reaction time. The products were analyzed by GC–MS and a wide range of compounds were detected via GC–MS chromatography during the catalytic oxydehydration of glycerol over 30PW/SBA-15(500). In comparison to glycerol, these newly formed compounds exhibited numerous substitutions of hydrogen and oxygen for carbon compounds ranging from C2 to C6. To optimize or standardize the process of converting glycerol to its corresponding oxydehydration products, it is crucial to understand and evaluate the mechanisms involved in the synthesis of these compounds from glycerol. Scheme 1 shows the proposed pathways for oxydehydration reaction of glycerol using the 30PW/SBA-15(500) catalyst.

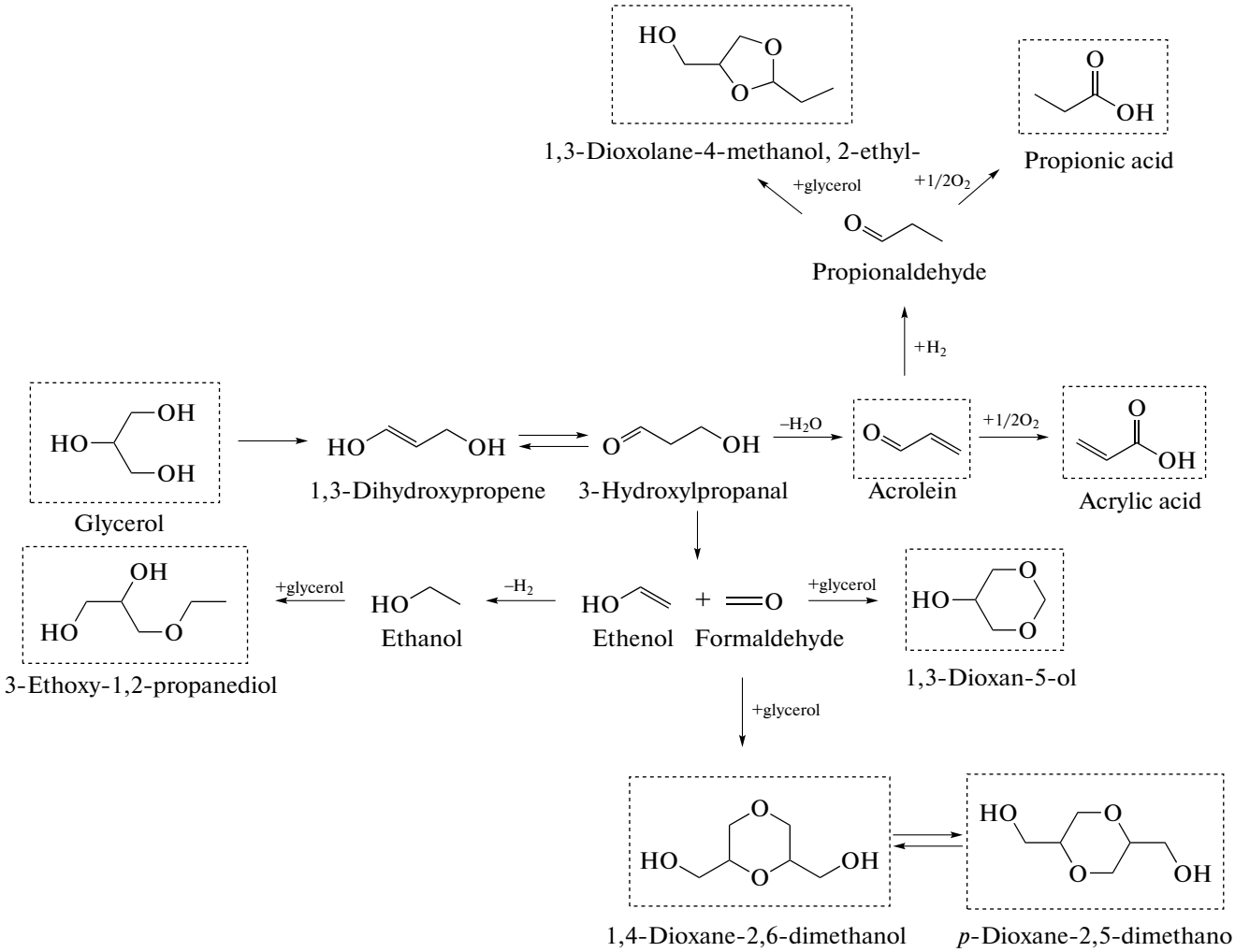

Scheme 1. Proposed pathways of the oxydehydration reaction of glycerol with the detected products represented by dashed lines.

Glycerol dehydration occurred only in the middle (or secondary) –OH groups when 30PW/SBA-15(500) was used. Acetol formation could not be observed since no acetol was detected during the dehydration process. In this pathway, the secondary glycerol –OH group is protonated, forming 1,3-dihydroxypropene by releasing a H_3O^+, followed by a keto-enol rearrangement to yield 3-hydroxypropanal [54]. Nevertheless, these species remained undetected due to their high reactivity. They promptly undergo a subsequent dehydration step, ultimately resulting in the formation of acrolein [55]. This glycerol dehydration seems to follow the reaction mechanism proposed by Alhanash et al. [56], who stated that direct protonation of the secondary glycerol –OH group is mainly catalyzed by Brønsted acidic sites. Acrolein eventually undergoes partial oxidation to acrylic acid with the assistance of redox sites on the 30PW/SBA-15(500) catalyst's surface (Scheme 1).

Furthermore, with the reaction progress, acrolein can also undergo hydrogenation to propionaldehyde [57], which readily reacts with unconverted glycerol to produce 1,3-dioxolane-4-methanol,2-ethyl- [58]. Glycerol acetals and ketals are among the promising chemicals that could be derived from glycerol reactions with various aldehydes. They are usually formed via heterogeneous acid catalysts such as supported HPAs. Additionally, this propionaldehyde can also undergo partial oxidation to form propionic acid [58]. In this study, proline-based heteropolyoxometalate $(ProH)_3[PW_{12}O_{40}]$ was effectively employed as a catalyst to selectively oxidize primary alcohols into their respective carboxylic acids, using H_2O_2 as the oxidizing agent.

Moreover, 3-hydroxypropanal can catalyze the cleavage of the C1–C2 bond, resulting in the formation of formaldehyde and ethenol through a retro-aldol reaction [7]. This formaldehyde can react with unconverted glycerol to form 1,3-dioxan-5-ol [59], which finds applications as a disinfectant and solvent for cosmetics and medical usage. Additionally, cyclic glycerol ethers (such as 1,4-dioxane-2,6-dimethanol and p-dioxane-2,5-dimethanol) were also identified in this reaction [60]. On the contrary, ethenol formed from retro-aldol reaction can undergo hydrogenation to produce ethanol. This ethanol eventually can react with unconverted glycerol in etherification reaction to produce 3-ethoxy-1,2-propanediol [61]. During this reaction, the protonation of glycerol on Brønsted acid sites leads to the generation of an oxone ion. Subsequently, this oxone ion reacts with ethanol, leading to the formation of mono ethyl glycerol ethers.

To summarize, the 30PW/SBA-15(500) catalyst exhibited excellent catalytic performance in converting glycerol through oxydehydration, resulting in high glycerol conversion and acrylic acid yield. Despite the catalyst exhibiting high selectivity towards acrylic acid, the presence of side reactions and subsequent oxidation resulted in the formation of various by-products. Nonetheless, due to the limitations in detecting or measuring certain intermediate products, determining the precise synthesis route for each compound derived from glycerol remains challenging. Consequently, it is possible to propose a hypothetical general reaction pathway, where certain paths are more or less feasible depending on the specific system under investigation.

Reaction Kinetics

The kinetic parameters such as the pre-exponential factor (A), reaction rate constant (k) and subsequently the activation energy (E_a), were also determined and summarized in Table 2. These values, determined at various temperatures, demonstrate a rising trend with increasing temperature. This trend aligns with the results reported by Thanasilp et al. [22]. Moreover, the pre-exponential factor (A) and activation energy (E_a) of the reaction were determined using the linear regression method, and the Arrhenius plot (Fig. 6).

The linearity of the plot of $\ln(k)$ vs. $1/T$ in in Fig. 6 confirms that the reaction follows an Arrhenius-type behavior, with a well-defined temperature dependence of the rate constant. Additionally, kinetic modeling based on experimental data indicated that a second-order rate law provides the best fit, suggesting that reversible dehydration of glycerol is negligible under studied conditions. Mechanistically, the second-order assumption is consistent with a rate-limiting bimolecular step involving glycerol and the catalyst surface, which aligns with prior studies on glycerol oxydehydration [22, 48]. Based on Fig. 6, the A and E_a values estimated were 4.742×10^{13} and 134.36 kJ/mol, respectively, with a good R^2 value of 0.97. Thus, the rate of glycerol oxydehydration can be expressed as below:

$$-r_{Gly} = 4.742 \times 10^{13} \exp\left(\frac{-134362}{8.3142T}\right) C_{Gly}^2. \qquad (7)$$

Thanasilp et al., reported an activation energy of 26.623 kJ/mol for the V6-SiW/HZSM-5 catalyst [22], which was comparably less active than the catalyst reported in this work. Although the activation energy determined in this study was higher than that reported

Table 2. Estimated rate constant values at different temperatures using 30PW/SBA-15(500)*

Temperature, °C	Estimated rate constant, L mol^{-1} h^{-1}
210	0.1271
220	0.3013
230	0.6201
240	0.8720

* Reaction conditions: catalyst loading 10 wt %, pressure 15–20 bar.

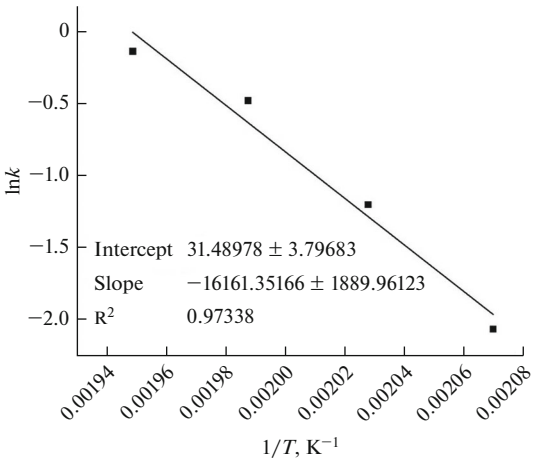

Fig. 6. Linearized Arrhenius equation plot.

in the previous research, it is crucial to note that the initial glycerol concentration employed here was substantially greater, potentially resulting in an elevated energy barrier. Moreover, it is crucial to take into account the influence of oxidizing agents and reaction temperatures on the activation energy as additional factors contributing to the process. In fact, in Ref. [22], H_2O_2 served as an oxidizing agent in the presence of catalysts under low reaction temperature.

Additionally, Fig. 7 illustrates the glycerol conversion profiles at four different reaction temperatures, providing a comparison between experimental and simulated results. The sum of squared errors (SSE) values for the kinetic model fitted to reaction temperatures of 210, 220, 230, and 240°C were 0.0664, 0.0323, 0.0102, and 0.0019, respectively. A lower SSE value indicates a smaller random error component in the model, thereby improving its predictive capability. The slightly higher SSE values observed at lower reaction temperatures suggest a less precise fit, indicating larger discrepancies between predicted and experimental data. Consequently, the reduced SSE values noted at reaction temperatures of 230 and 240°C signify an enhanced model fit to experimental data at those temperatures. This highlights the applicability of the pseudo-second-order kinetic model for evaluating

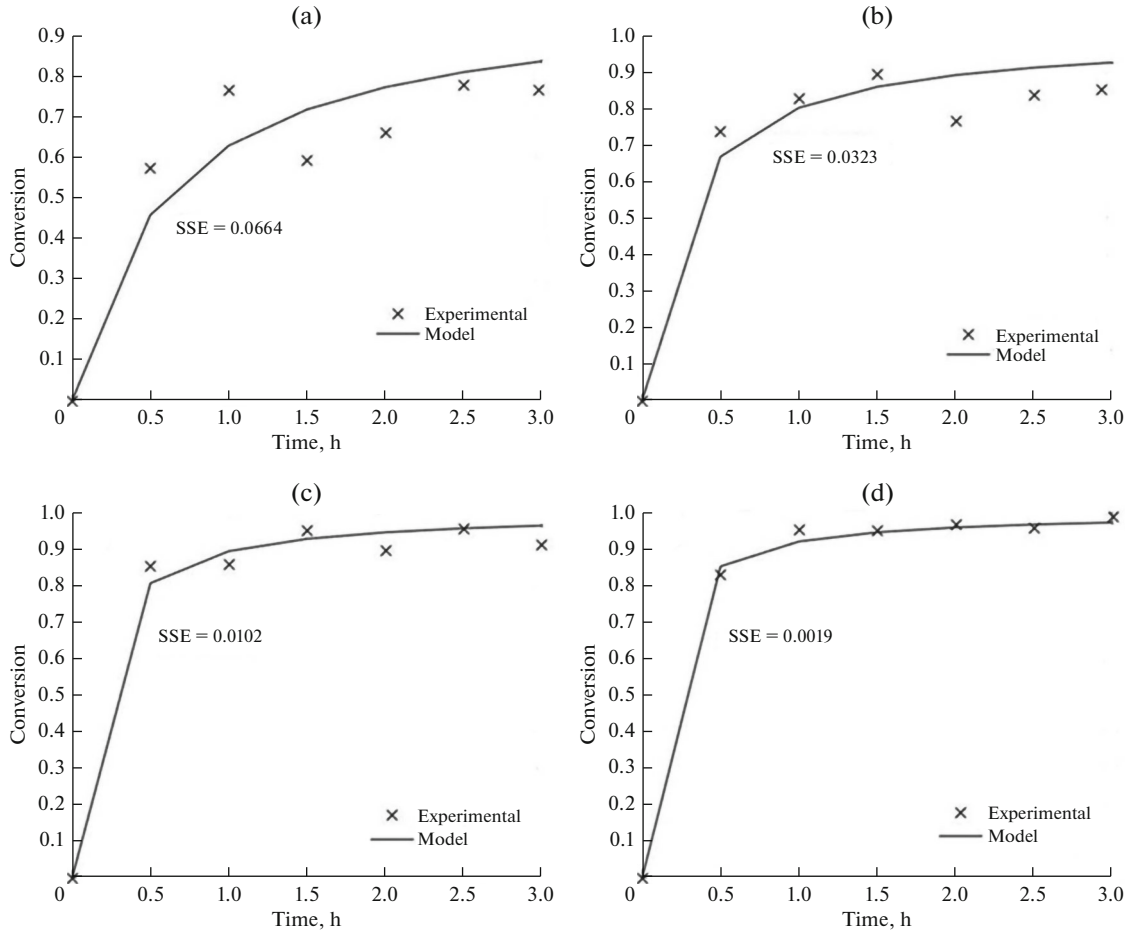

Fig. 7. Comparison between simulated and experimental glycerol conversions at various reaction temperatures: 210 (a), 220 (b), 230 (c), and 240°C (d).

glycerol oxydehydration reactions, particularly within higher temperature ranges.

CONCLUSIONS

In this study, the 30PW/SBA-15(500) catalyst, prepared with 30 wt % HPW and calcined at 500°C, exhibited favorable catalytic performance. Increasing HPW loading up to 30 wt % enhanced activity, while further increases caused a decline. Higher calcination temperatures reduced catalyst acidity and, consequently, catalytic activity toward glycerol oxydehydration. Optimal conditions were a 3-h reaction at 240°C with 10 wt % catalyst-to-glycerol loading, achieving 98.7% glycerol conversion and 22.2% acrylic acid yield using the 30PW/SBA-15(500) catalyst. The proposed reaction mechanism involves catalytic dehydration of glycerol to acrolein via Brønsted acid sites, followed by partial oxidation facilitated by redox sites. The glycerol oxydehydration kinetics follow a pseudo second-order model with an activation energy of 134.36 kJ/mol. This kinetic model accurately predicts reaction data, especially at temperatures above 230°C.

ABBREVIATIONS AND NOTATION

HPA	heteropoly acid
HPW	heteropoly phosphotungstic acid
X	glycerol conversion
Y	product yield
S	selectivity
k	reaction rate constant
E_a	activation energy
A	pre-exponential factor
SSE	sum of squared errors.

AUTHOR CONTRIBUTION

Muhammad Yusri Ahmad: methodology and investigation, writing-original draft preparation; Syamima Nasrin Mohamed Saleh: data curation, validation; Anwar Ul-Hamid: resources, writing-review; Ahmad Zuhairi Abdullah: resources, funding, editing, supervision.

FUNDING

The Fundamental Research Grant Scheme (FRGS/1/2021/TK0/USM/01/2) from the Ministry of Higher Education Malaysia to support this project is acknowledged.

DATA AVAILABILITY

The data presented in this study are available upon request.

CONFLICT OF INTEREST

The authors of this work declare that they have no conflict of interest.

REFERENCES

1. Stipp, H., Market volume of acrylic acid worldwide from 2015 to 2022, with a forecast for 2023 to 2030. https://www.statista.com/statistics/1245262/acrylic-acid-market-volume-worldwide. Accessed 2023.
2. Ahmad, M.Y., Basir, N.I., and Abdullah, A.Z., *J. Ind. Eng. Chem.,* 2021, vol. 93, p. 216. https://doi.org/10.1016/j.jiec.2020.09.026
3. Mestl, G. Margitfalvi, J.L., Végvári, L., SzijjártóG., P., and Tompos, A., *Appl. Catal. A Gen.,* 2014, vol. 474, p. 3. https://doi.org/10.1016/j.apcata.2013.08.022
4. Brazdil, J.F., *Appl. Catal. A: Gen.,* 2017, vol. 543, p. 225. https://doi.org/10.1016/j.apcata.2017.06.022
5. Li, C., Zhu, Q., Cui, Z., Wang, B., Fang, Y., and Tan, T., *Chem. Eng. Sci.,* 2018, vol. 183, p. 288. . https://doi.org/10.1016/j.ces.2018.03.030
6. Zhang, X., Lin, L., Zhang, T., Liu, H., and Zhang, X., *Chem. Eng. J.,* 2016, vol. 284, p. 934. https://doi.org/10.1016/j.cej.2015.09.039
7. Lopez-Pedrajas, S., Estevez, R., Schnee, J., Gaigneaux, E.M., Luna, D., and Bautista, F.M., *Mol. Catal.,* 2018, vol. 455, p. 68. https://doi.org/10.1016/j.mcat.2018.05.020
8. Wang, F., Dubois, J.L., and Ueda, W., *Appl. Catal. A: Gen.,* 2010, vol. 376, p. 25. https://doi.org/10.1016/j.apcata.2009.11.031
9. Wang, F., Dubois, J.L., and Ueda, W., *J. Catal.,* 2009, vol. 268, p. 260. https://doi.org/10.1016/j.jcat.2009.09.024
10. Deleplanque, J., Dubois, J.L., Devaux, J.F., and Ueda, W., *Catal. Today,* 2010, vol. 157, p. 351. https://doi.org/10.1016/j.cattod.2010.04.012
11. Chieregato, A., Basile, F., Concepción, P., Guidetti, S., Liosi, G., Soriano, M.D., Trevisanut, C., Cavani, F., and Nieto, J.M.L., *Catal. Today,* 2012, vol. 197, p. 58. https://doi.org/10.1016/j.cattod.2012.06.024
12. Omata, K., Matsumoto, K., Murayama, T., Ueda, W., *Catal. Today,* 2016, vol. 259, p. 205. https://doi.org/10.1016/j.cattod.2015.07.016
13. Possato, L.G., Cassinelli, W.H., Meyer, C.I., Garetto, T., Pulcinelli, S.H., Santilli, C.V., and Martins, L., *Appl. Catal. A: Gen.,* 2017, vol. 532, p. 1. https://doi.org/10.1016/j.apcata.2016.12.010
14. Rasteiro, L.F., Vieira, L.H., Possato, L.G., Pulcinelli, S.H., Santilli, C.V., and Martins, L., *Catal. Today,* 2017, vol. 296, p. 10. https://doi.org/10.1016/j.cattod.2017.04.006
15. Shen, L., Yin, H., Wang, A., Lu, X., and Zhang, C., *Chem. Eng. J.,* 2014, vol. 244, p. 168. https://doi.org/10.1016/j.cej.2014.01.051
16. Soriano, M.D., Concepción, P., Nieto, J.M.L., Cavani, F., Guidetti, S., and Trevisanut, C., *Green Chem.,* 2011, vol. 13, p. 2954. https://doi.org/10.1039/c1gc15622e
17. Arcanjo, M.A., Silva, I.J., Jr., Rodriguez-Castellon, E., Infantes-Molina, A., and Vieira, R.S., *Catal. Today,* 2017,

vol. 279, p. 317.
https://doi.org/10.1016/j.cattod.2016.02.015

18. Diallo, M.M., Mijoin, J., Laforge, S., and Pouilloux, Y., *Catal. Commun.,* 2016, vol. 79, p. 58.
https://doi.org/10.1016/j.catcom.2016.03.003
19. dos Santos, M.B., Andrade, H.M.C., and Mascarenhas, A.J.S., *Micropor. Mesopor. Mater.,* 2019, vol. 278, p. 366.
https://doi.org/10.1016/j.micromeso.2019.01.016
20. Possato, L.G., Chaves, T.F., Cassinelli, W.H., Pulcinelli, S.H., Santilli, C.V., and Martins, L., *Catal. Today,* 2017, vol. 289, p. 20.
https://doi.org/10.1016/j.cattod.2016.08.005
21. Liu, L., Wang, B., Du, Y., Zhong, Z., and Borgna, A., *Appl. Catal. B: Environ.,* 2015, vols. 174–175, p. 1.
https://doi.org/10.1016/j.apcatb.2015.02.032
22. Thanasilp, S., Schwank, J.W., Meeyoo, V., Pengpanich, S., and Hunsom, M., *Chem. Eng. J.,* 2015, vol. 275, p. 113.
https://doi.org/10.1016/j.cej.2015.04.010
23. Thanasilp, S., Schwank, J.W., Meeyoo, V., Pengpanich, S., and Hunsom, M., *J. Mol. Catal. A Chem.,* 2013, vol. 380, p. 49.
https://doi.org/10.1016/j.molcata.2013.09.023
24. Wang, G., Li, Z., and Li, C., *Chem. Eng. Sci.,* 2022, vol. 247, p. 117052.
https://doi.org/10.1016/j.ces.2021.117052
25. Ahmad, M.Y., Saleh, S.N.M., and Abdullah, A.Z., *Appl. Catal. A: Gen.,* 2024, vol. 670, p. 119534.
https://doi.org/10.1016/j.apcata.2023.119534
26. Saleh, S.N.M. and Abdullah, A.Z., *Waste Biomass Valor.,* 2020, vol. 12, p. 2565.
https://doi.org/10.1007/s12649-020-01200-4
27. Shen, L., Yin, H., Wang, A., Lu, X., Zhang, C., Chen, F., Wang, Y., and Chen, H., *J. Ind. Eng. Chem.,* 2014, vol. 20, p. 759.
https://doi.org/10.1016/j.jiec.2013
28. Saleh, S.N.M., Ahmad, M.Y., Ul-Hamid, A., and Abdullah, A.Z., *Powder Tech.,* 2024, vol. 444, p. 120048.
https://doi.org/10.1016/j.powtec.2024.120048
29. Kojima, K., Osuga, R., Yasuda, S., Yokoi, T., Hosogi, Y., Itagaki, S., Okumura, Y., and Kondo, J.N., *J. Catal.,* 2021, vol. 395, p. 387.
https://doi.org/10.1016/j.jcat.2021.01.011
30. Shen, H., Li, Y., Huang, S., Cai, K., Cheng, Z., Lv, J., and Ma, X., *Catal. Today,* 2019, vol. 330, p. 117.
https://doi.org/10.1016/j.cattod.2018.04.001
31. Hoo, P.Y. and Abdullah, A.Z., *Chem. Eng. J.,* 2014, vol. 250, p. 274.
https://doi.org/10.1016/j.cej.2014.04.016
32. Zhao, D., Feng, J., Huo, Q., Melosh, N., Fredrickson, G.H., Chmelka, B.F., and Stucky, G.D., *Science,* 1998, vol. 279, p. 548.
https://doi.org/10.1126/science.279.5350.548
33. Janssen, A.H., van Der Voort, P., Koster, A.J., and De Jong, K.P., *Chem. Commun.,* 2002, vol. 2, p. 1632.
https://doi.org/10.1039/b204943k
34. Frattini, L., Isaacs, M.A., Parlett, C.M.A., Wilson, K., Kyriakou, G., and Lee, A.F., *Appl. Catal. B: Environ.,* 2017, vol. 200, p. 10.
https://doi.org/10.1016/j.apcatb.2016.06.064
35. Chong, C.C., Aqsha, A., Ayoub, M., Sajid, M., Abdullah, A.Z., Yusup, S., and Abdullah, B., *Environ. Technol. Innov.,* 2020, vol. 19, p. 100859.
https://doi.org/10.1016/j.eti.2020.100859
36. Brahmkhatri, V. and Patel, A., *Appl. Catal. A: Gen.,* 2011, vol. 403, p. 161.
https://doi.org/10.1016/j.apcata.2011.06.027
37. Essayem, N., Holmqvist, A., Gayraud, P.Y., Vedrine, J.C., and Taarit, Y.B., *J. Catal.,* 2001, vol. 197, p. 273.
https://doi.org/10.1006/jcat.2000.310
38. Rao, R.G. and Rajkumar, T., *Catal. Lett.,* 2008, vol. 120, p. 261.
https://doi.org/10.1007/s10562-007-9279-2
39. Rao, R.G. and Rajkumar, T., *J. Colloid Interface Sci.,* 2008, vol. 324, p. 134.
https://doi.org/10.1016/j.jcis.2008.04.070
40. Atia, H., Armbruster, U., and Martin, A., *J. Catal.,* 2008, vol. 258, p. 71.
https://doi.org/10.1016/j.jcat.2008.05.027
41. Talebian-Kiakalaieh, A. and Amin, N.A.S., *Catal. Today,* 2015, vol. 256, p. 315.
https://doi.org/10.1016/j.cattod.2015.01.045
42. Gagea, B.C., Lorgouilloux, Y., Altintas, Y., Jacobs, P.A., and Martens, J.A., *J. Catal.,* 2009, vol. 265, p. 99.
https://doi.org/10.1016/j.jcat.2009.04.017
43. Okoye, P.U., Abdullah, A.Z., and Hameed, B.H., *J. Taiwan Inst. Chem. Eng.,* 2016, vol. 68, p. 51.
https://doi.org/10.1016/j.jtice.2016.09.011
44. Chen, A.J., Chen, X.R., and Mou, C.Y., *J. Chin. Chem. Soc.,* 2010, vol. 57, p. 820.
https://doi.org/10.1002/jccs.201000114
45. Yang, L., Qi, Y., Yuan, X., Shen, J., and Kim, J., *J. Mol. Catal. A Chem.,* 2005, vol. 229, p. 199.
https://doi.org/10.1016/j.molcata.2004.11.024
46. Southward, B.W.L., Vaughan, J.S., and O'Connor, C.T., *J. Catal.,* 1995, vol. 153, p. 293.
https://doi.org/10.1006/jcat.1995.1131
47. Kozhevnikov, I.V., *Chem. Rev.,* 1998, vol. 98, p. 171.
https://doi.org/10.1021/cr960400y
48. Possato, L.G., Acevedo, M.D., Padró, C.L., Briois, V., Passos, A.R., Pulcinelli, S.H., Santilli, C.V., and Martins, L., *Mol. Catal.,* 2020, vol. 481, p. 110158.
https://doi.org/10.1016/j.mcat.2018.07.029
49. Suganuma, S., Hisazumi, T., Taruya, K., Tsuji, E., and Katada, N., *Mol. Catal.,* 2018, vol. 449, p. 85.
https://doi.org/10.1016/j.mcat.2018.02.015
50. Sánchez, N., Martínez, M., and Aracil, J., *Ind. Eng. Chem. Res.,* 1997, vol. 36, p. 1524.
https://doi.org/10.1021/ie9603124
51. Marchetti, J.M. and Errazu, A.F., *Biomass Bioenerg.,* 2008, vol. 32, p. 892.
https://doi.org/10.1016/j.biombioe.2008.01.001
52. Lacerda, L.C.T., Dos Santos, P.M., Corrêa, S., Oliveira, L.C.A., and Ramalho, T.C., *Chem. Phys. Lett.,* 2016, vol. 651, p. 161.
https://doi.org/10.1016/j.cplett.2016.03.038
53. Li, X. and Zhang, Y., *ACS Catal.,* 2016, vol. 6, p. 2785.
https://doi.org/10.1021/acscatal.6b00213
54. Abdullah, A., Abdullah, A.Z., Ahmed, M., Khan, J., Shahadat, M., Umar, K., and Alim, M.A., *J. Cleaner*

Prod., 2022, vol. 341, p. 130876. https://doi.org/10.1016/j.jclepro.2022.130876

55. Katryniok, B., Paul, S., and Dumeignil, F., *ACS Catal.,* 2013, vol. 3, p. 1819. https://doi.org/10.1021/cs400354p
56. Alhanash, A., Kozhevnikova, E.F., and Kozhevnikov, I.V., *Appl. Catal. A: Gen.,* 2010, vol. 378, p. 11. https://doi.org/10.1016/j.apcata.2010.01.043
57. Gong, H., Zhou, C., Cui, Y., Dai, S., Zhao, X., Luo, R., An, P., Li, H., Wang, H., and Hou, Z., *ChemSusChem,* 2020, vol. 13, p. 4954. https://doi.org/10.1002/cssc.202001600
58. Chen, L., Nohair, B., Zhao, D., and Kaliaguine, S., *ChemCatChem,* 2018, vol. 10, p. 1918. https://doi.org/10.1002/cctc.201701656
59. Li, R., Song, H., and Chen, J., *Catalysts,* 2018, vol. 8, p. 8080297. https://doi.org/10.3390/catal8080297
60. Zhou, K., Sun, C., and Liu, X., *Chem. Eng. J.,* 2022, vol. 430, p. 132981. https://doi.org/10.1016/j.cej.2021.132981
61. Palanychamy, P., Lim, S., Yap, Y.H., and Leong, L.K., *Catalysts,* 2022, vol. 12, p. 12111487. https://doi.org/10.3390/catal12111487